Geophys. J. Int. (2004) **156,** 59–72 doi: 10.1111/j.1365-246X.2004.02127.x

Thickness and V_p/V_s Ratio Variation in the Iberian Crust

Jordi Julià[1] and Jorge Mejía[2]

[1]*Department of Geosciences, Penn State University, University Park, Pennsylvania, USA. E-mail: jjulia@geosc.psu.edu*
[2]*Observatorio Simológico del Sur-Occidente, Universidad del Valle, Cali, Valle, Colombia. E-mail: jmm@osso.org.co*

Accepted 2003 September 10. Received 2003 September 1; in original form 2003 January 2

SUMMARY

Local estimates of crustal thickness and V_P/V_S ratio across the Iberian Peninsula have been obtained from the stacking of teleseismic *P*-to-*S* converted waves and multiply reverberated waves at the crust–mantle boundary. The stacking procedure requires an *a priori* knowledge of the bulk *P*-wave velocity of the crust, which has been obtained by averaging independent seismic profiling velocity models. The thicknesses and V_P/V_S ratios reported in this work fit well within the tectonic framework operating in the region, and clearly image features such as the crustal roots at the Pyrenees and Catalan Coastal Ranges, and the stretched crust in the València Trough. Our analysis also confirms the presence of an uppermost mantle velocity contrast east of the Palomares Fault. In the Iberian Massif, our results indicate that the thickness of the crust (30 ± 2 km) is lower than expected for a continental crust of Palaeozoic age. The possibility of removal of mafic lower crust could not be assessed from the corresponding V_P/V_S average in this unit (1.74 ± 0.05). Our estimates agree with seismic profiling estimates and extend those results with local estimates for thickness and V_P/V_S ratio at 11 sites in Iberia.

Key words: continental crust, Iberian Peninsula, Poisson's ratio, receiver function.

GJI Seismology

1 INTRODUCTION

Seismic characterization of the crust has most commonly been achieved with seismic velocities and thicknesses, as reported by seismic profiling. A significant number of refraction lines have sampled the crust of the Iberian Peninsula, and have reported crustal thicknesses and *P*-wave velocities (e.g. Banda & Ansorge 1980; Banda *et al.* 1980; Gallart *et al.* 1981) across Spain and Portugal. More recently, reflection surveys have also added valuable information to the crustal characterization of Iberia (e.g. Gallart *et al.* 1995; Carbonell *et al.* 2001). Earth models proposed from these works show some interesting features for the Iberian crust and upper-mantle. The Iberian Massif, for instance, is characterized by a 32 km thick crust (Banda 1988), which is lower than expected for Palaeozoic orogens (Zandt & Ammon 1995). Also, the lower crust in the Ebre Basin and the Pyrenees have been imaged as a layer with a rather low 6.4 km s^{-1} velocity (Gallart *et al.* 1981, 1995), which contrasts with values of 6.7–6.8 km s^{-1} reported for the Iberian Massif. In the upper-mantle, a 63 km deep reflector has also been reported beneath south–east Spain, as part of a low-velocity zone in the upper-mantle (Banda & Ansorge 1980; Mueller & Ansorge 1986). Occasionally, seismic profiling provides *S*-wave velocity information (e.g. Banda *et al.* 1981), but this information is generally scarce.

Teleseismic receiver functions (Langston 1979) have proven to be a useful tool for estimating crustal thicknesses and V_P/V_S ratios beneath individual seismic stations (e.g. Zandt *et al.* 1995; Chevrot & Van der Hilst 2000; Zhu & Kanamori 2000). The *P*-to-*S* converted phase at the Moho and the first multiply reverberated phases in the crust are generally apparent in the receiver function waveforms, and their relative traveltimes can then be employed to constrain the thickness and the V_P/V_S below the recording station (Zandt & Ammon 1995). The aim of this study is to analyse receiver functions in the Iberian Peninsula, in order to extend the characterization of the bulk seismic properties of the Iberian crust with local estimates for thickness and V_P/V_S ratio. To this purpose, we apply the stacking procedure of Zhu & Kanamori (2000) to 11 seismic stations located in the Iberian Peninsula. This procedure is reviewed, and estimates for the V_P/V_S ratios and thicknesses of the whole crust are then reported, compared with independent studies, and discussed within their corresponding tectonic setting. Our results agree with previous seismic profiling studies, provide new V_P/V_S ratio and thickness estimates and fit within the tectonic framework operating in the Iberian–Mediterranean region.

2 TECTONIC FRAMEWORK

The Iberian Peninsula can be viewed as a relatively undeformed Palaeozoic core, the Iberian Massif, surrounded by areas that have undergone Alpine deformation (Fig. 1). The Iberian Massif is the largest outcrop of the European Variscan lithosphere and contains the Mesozoic Lusitanian Basin to the west, and the Central System, which is an uplifted outcrop of the Palaeozoic basement separating two Neogen basins (Duero and Tajo). To the south is the Betic Cordillera, which is a Neogene fold belt (Weijermars 1991), although it has also been regarded as a straightforward product of the collision between the Iberian and African plates by some

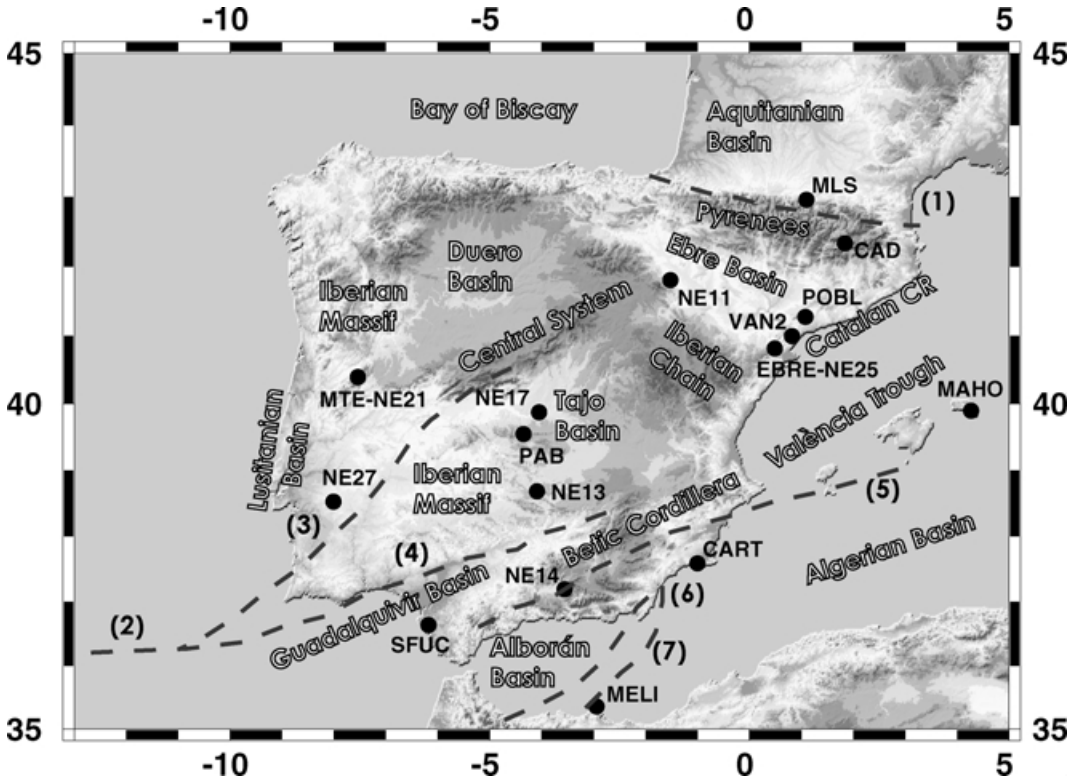

Figure 1. The main tectonic units and seismic stations in Iberia. Circles indicate stations considered for this study. Dashed lines indicate strike-slip faults: (1) North Pyrenean, (2) Açores Fault, (3) Plasencia Lineament, (4) Guadalquivir Lineament, (5) Crevillente Fault, (6) Palomares Fault and (7) Nekor Fault (from Weijermars 1991).

authors (e.g. Dewey *et al.* 1973). The Betics are separated from the Iberian Massif by the Guadalquivir foreland basin. To the north, the Pyrenees, which are part of the Alpine chain of Western Europe, are considered a shortened crustal domain that occupies the site of the boundary between separate Iberian and European plates during Cretaceous times (Choukroune 1992). The Aquitanian and Ebre basins are its northern and southern foreland basins, respectively. The Ebre Basin is separated from the Iberian Massif by the Iberian Cordillera, which is sometimes interpreted as the Alpine deformation of a former thinned crust of the Celtiberian aulacogen (Álvaro *et al.* 1979). To the east, Neogen extension in the western Mediterranean originated the opening of the València Trough, the Provençal–Algerian Basin and its westward projection, the Alborán Basin.

The units outlined above are the result of the tectonic interaction of Iberia with the surrounding Eurasian and African plates since Mesozoic times. Vegas & Banda (1982) arranged these interactions in time along three major stages: continental rifting (230–80 Ma), convergence (50–15 Ma) and extension off the Mediterranean margin (20–0 Ma). The rifting stage was circumscribed by the breakup of Pangea and opening of the Atlantic ocean, and by extensional processes in the Western Mediterranean (Sanz de Galdeano 1995). It was during this stage that the opening of the Bay of Biscay (with production of oceanic crust) took place and the Lusitanian Basin started to develop. The second stage—NS convergence between Africa and Iberia—began at early Tertiary times, eventually bringing about subduction and, by Early Eocene, ending up in collision. The Eocene compression was transmitted to the entire Iberian plate causing deformation at the Pyrenees and Catalan Coastal Ranges (CCR), subduction of the oceanic crust in the Bay of Biscay beneath Iberia, and crustal thickening in the Central System. The third stage developed during the Oligocene, when EW extension in the Western Mediterranean compressed the eastern section of Iberia. This affected the Iberian Cordillera and the Central System, and the Duero and Tajo basins formed. The extension continued through the Neogene with the opening of the Provençal Basin, which extended southwards to the Algerian Basin and eventually reached the Alborán Basin by Early Miocene. The internal zones of the Betic Cordillera were accreted to SE Iberia at this time, deforming the Betics external zones and developing the Guadalquivir Basin. Details of the Mesozoic–Cenozoic evolution described in this paragraph can be found, for example, in Uchupi (1988) and Sanz de Galdeano (1995) and the references therein.

In summary, the western margin of Iberia has evolved as a passive margin since the opening of the central Atlantic, the northern border became inactive after the creation of the Pyrenees (although some activity is still present) and the eastern margin became a broad intracontinental collision zone subsequently dismembered by the formation of the western Mediterranean basins (Vegas & Banda 1982). The southern border is indeed part of the present plate margin between Eurasia and Africa, but its precise location is still the subject of debate (see, e.g., Stich *et al.* 2003). How extension in the western Mediterranean has developed within a global regime of compression is still unclear, although a region of large-scale mantle upwelling from combined seismic tomography, isotope geochemistry and regional geology data has been postulated (Hoernle *et al.* 1995) to unravel this problem. The Palaeozoic core of Iberia, the Iberian Massif, has been relatively undeformed since the Mesozoic and can be regarded as a tectonically stable region of Iberia.

3 RECEIVER FUNCTION STACKING AND CONFIDENCE BOUNDS

Receiver functions are time-series containing Ps converted and multiply reverberated phases generated at seismic discontinuities beneath the recording station. In practice, receiver functions are obtained by deconvolving the vertical component from the horizontal components in the time window corresponding to the teleseismic *P*-wave coda (Langston 1979). As a result of the steep incidence of the incoming teleseismic *P*-wave, the resulting particle motion is polarized so that *S*-waves are preferentially recorded in the radial component and *P*-waves in the vertical component. The combination of this property with the deconvolution process, makes the radial receiver function a scaled version of the radial component of the displacement with the removal of phases with a final *P*-wave leg (Ammon 1991). Moreover, when the propagating medium under the stations is laterally homogeneous, the transverse receiver function must be identically zero. Therefore, computing transverse receiver functions provides some testing for the signature of laterally varying media or small 3-D heterogeneities in the radial receiver functions.

Receiver functions have been employed to obtain detailed *S*-wave velocity structure in the crust and upper-mantle (Owens *et al.* 1984; Ammon *et al.* 1990). In general, those studies assume an *a priori* value for the V_P/V_S ratio. Zandt *et al.* (1995) noted that the relative traveltimes for the Ps, PpPms and PpSms+PsPms phases can be employed to constrain the thickness and the V_P/V_S ratio of the crust, provided that the *P*-wave velocity is known. They applied their methodology at 10 broad-band stations deployed along the Basin and Range-Colorado Plateau transect to report crustal thickness variations and V_P/V_S of the crust along the profile. Recently, Zhu & Kanamori (2000) devised a receiver function stacking technique to obtain average V_P/V_S ratios and crustal thicknesses beneath seismic stations. Their methodology consists of a transformation from a time domain representation of the receiver functions into a new domain which is a function of the depth of the interface H and the V_P/V_S ratio. This is described as

$$\mathrm{s}(H,\kappa) = \sum_j w_1 \mathrm{rf}_j(t_1) + w_2 \mathrm{rf}_j(t_2) - w_3 \mathrm{rf}_j(t_3)., \quad (1)$$

where H is thickness, κ is the V_P/V_S ratio, $\mathrm{rf}_j(t)$ are the receiver functions, with j ranging from 1 to the total number of waveforms, w_i are *a priori* weights such that $\sum w_i = 1$, and the t_i are given by

$$\begin{aligned} t_1 &= t_{Ps} - t_P = H(\eta_\beta - \eta_\alpha) \\ t_2 &= t_{\mathrm{PpPms}} - t_P = H(\eta_\beta + \eta_\alpha) \\ t_3 &= t_{\mathrm{PpSms}} - t_P = 2H\eta_\beta \end{aligned} \quad (2)$$

where H is thickness and η is vertical slowness. During the transformation, coherent phases are constructively superposed while non-coherent signals tend to be eliminated if the number of records is large enough. In fact, seismic phases such as Ps, PpPms and PpSms+PsPms will add constructively only when the assumed depth of the reflector and the V_P/V_S ratio coincide with the actual values underneath the station. An approximate value of the *P*-wave

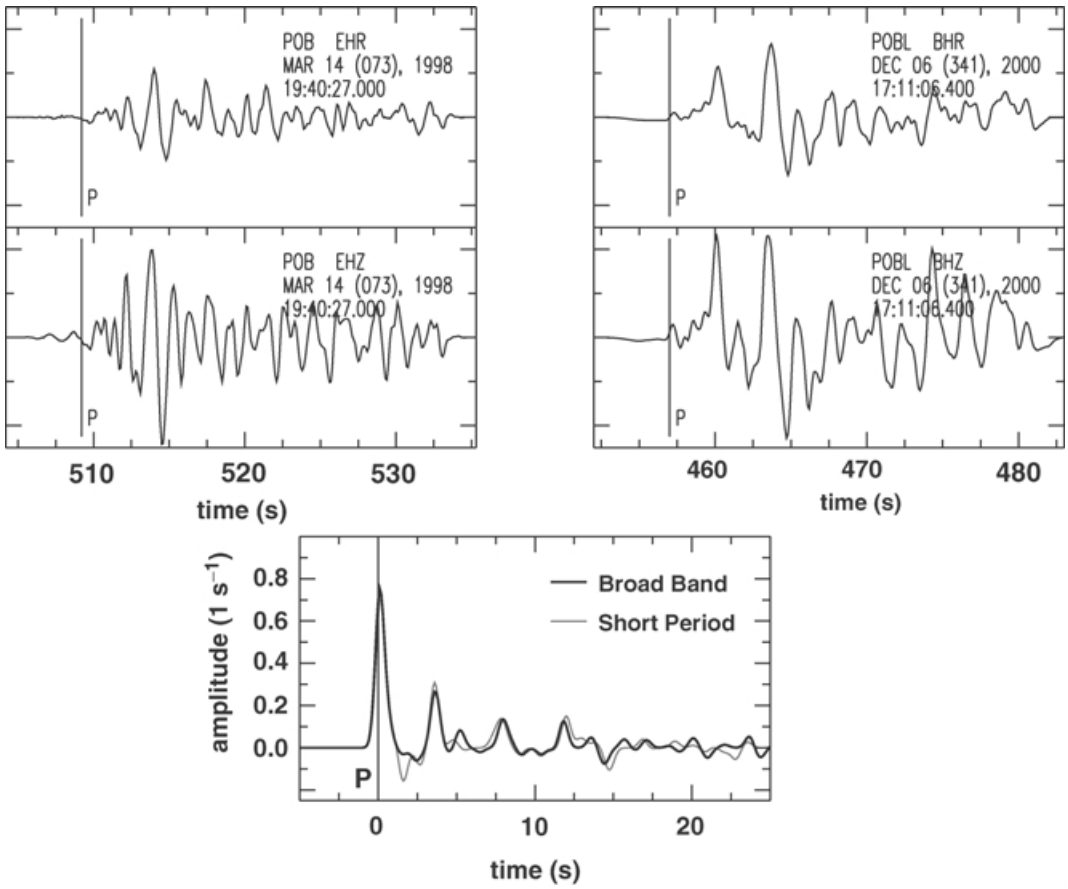

Figure 2. Vertical and radial waveforms at POBL, as recorded by Ranger-SS1 (left) and STS2 (right) sensors. An overlap of the deconvolved traces is shown at the bottom. Small differences in the Ps and multiples are caused by slightly different ray parameters, but the similarity is striking.

velocity has to be assumed prior to the stacking, and the location of the maximum in the stacking surface, therefore, provides the estimates for H and V_P/V_S. Since the new domain is independent of ray parameter, this technique allows us to stack directly the H–κ representation of all the available records provided that the medium is laterally homogeneous and isotropic.

3.1 Limitations of the H–κ stacking

One implicit assumption in the development of eq. (2) is that the Moho is a planar, horizontal interface (Zandt *et al.* 1995). Dipping of this interface will affect the Poisson ratio estimates. Multiples travelling updip will travel larger distances through the crust and will have longer relative traveltimes, with respect to those generated at a horizontal interface (Ligorría 2000). Conversely, multiples travelling downdip will have shorter relative traveltimes. As a result, waves travelling updip will underestimate the value of the Poisson ratio and waves travelling downdip will overestimate that value. This effect might be significant in regions of rapid crustal thickness variations, such as the Catalan Coastal Ranges–València Trough transition.

Even when the isotropic, laterally homogeneous medium hypothesis holds, there are situations in which the stacking procedure may fail. One of these situations is the presence of a gradational crust–mantle boundary instead of a sharp, well-defined Moho discontinuity. A gradational crust–mantle transition makes the energy from the boundary interaction phases spread in time, so that the corresponding pulses decrease in amplitude and increase in width (Cassidy 1992; Ligorría 2000). This effect is stronger in the multiples compared with the Ps converted phase, since the multiples follow longer ray-paths through the medium and the multiply reverberated phases become more likely to be contaminated—or even masked—by the background scattering. Because of the depth–velocity trade-off (Ammon *et al.* 1990) the stacking analysis requires at least two phases to be identified in the waveforms. If the multiples are masked, then the resulting constraints are weak.

Another tricky situation arises when the Moho Ps converted phase interferes with multiples from an intracrustal discontinuity. This is a common situation in sedimentary environments, where the multiples from the sediment–bedrock interface overlap in time with the Ps converted phase at the Moho (Cassidy 1992; Zelt & Ellis 1998). The interference may cause a time-shift of the Ps peak that, when combined with the multiples from the Moho, may lead to unrealistic estimates of thickness and V_P/V_S ratios. The ringing caused by the reverberations of energy trapped in the sedimentary cover

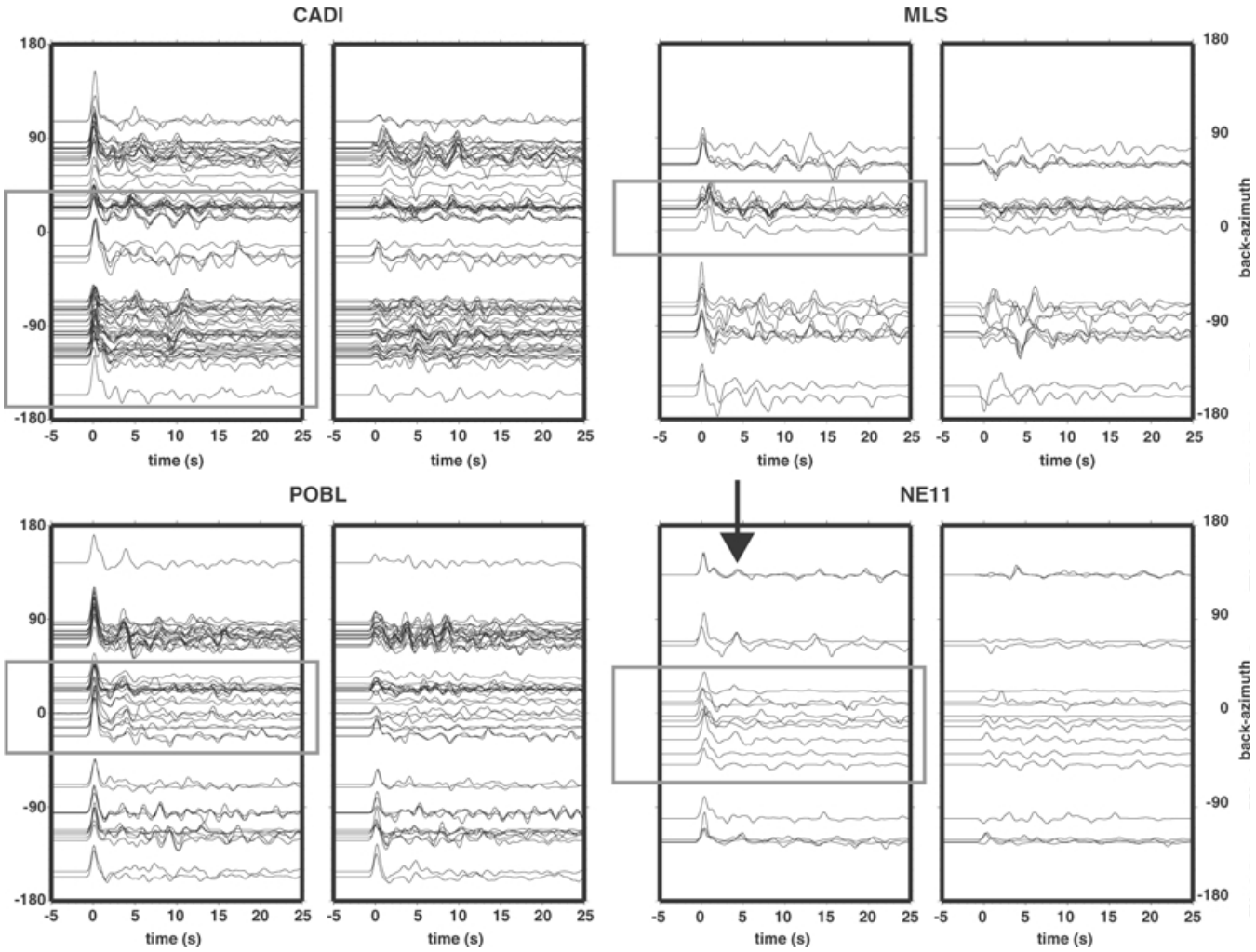

Figure 3. Radial and transverse receiver functions in the Pyrenees, Aquitanian Basin and Ebre Basin. Note the varying patterns for the eastern, northern and western backazimuths, respectively. The rectangles indicate the range of backazimuths used in the H–κ stacking. The arrow points to the Moho Ps converted phase at station NE11.

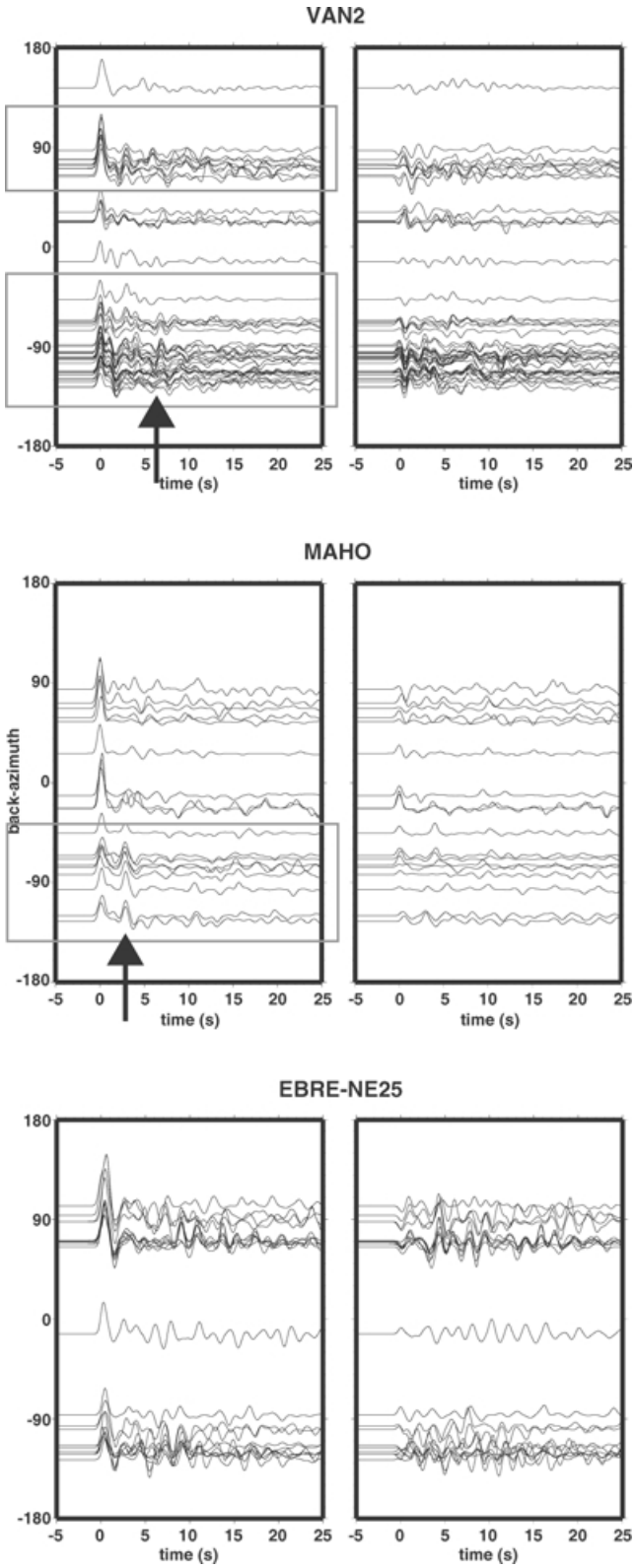

Figure 4. Radial and transverse receiver functions in the Catalan Coastal Ranges and València Trough. Note the varying patterns at the short-period station VAN2 for the eastern (CCR), and western (trough) backazimuths, respectively. The arrows point to specific features in the waveforms referenced in the text.

may even extend far enough in time to overlap with Moho multiples (Zelt & Ellis 1998; Julià *et al.* 2003). In this case, little information concerning the whole crust can be recovered from the receiver functions without sophisticated processing of a large distributed set of data. However, when the ringing only affects the Ps phase, the multiples can still be used to learn about the average properties of the crust.

3.2 Correlation and uncertainties

Zhu & Kanamori (2000) obtain confidence limits for the estimated values of V_P/V_S ratios and thickness by using the flatness of the stacking surface. According to the authors, the variance for the thickness σ_H^2 and the V_P/V_S ratio σ_k^2 are

$$\sigma_H^2 = 2\sigma_s \Big/ \frac{\partial^2 s}{\partial H^2}$$
$$\sigma_\kappa^2 = 2\sigma_s \Big/ \frac{\partial^2 s}{\partial \kappa^2}, \tag{3}$$

where σ_s is the estimated variance of s(H, κ) from stacking (eq. 1). These equations assume that there is no correlation between the crustal thickness and V_P/V_S ratio. However, because of the depth–velocity trade-off, a strong, negative correlation should be expected. Since V_P is kept constant during the analysis, traveltimes can always be preserved by increasing V_S—decreasing V_P/V_S—upon increasing H and vice versa. The stacking surface (eq. 1) can be better approximated using a bivariate Gaussian distribution, and the expressions for the variances σ_H^2 and σ_κ^2 and the covariance $\sigma_{H\kappa}$ become

$$\sigma_H^2 = 2\sigma_s \frac{\partial^2 s}{\partial \kappa^2} \Big/ \left(\frac{\partial^2 s}{\partial H^2}\frac{\partial^2 s}{\partial \kappa^2} - \frac{\partial^2 s}{\partial \kappa \partial H}\frac{\partial^2 s}{\partial \kappa \partial H} \right)$$
$$\sigma_\kappa^2 = 2\sigma_s \frac{\partial^2 s}{\partial H^2} \Big/ \left(\frac{\partial^2 s}{\partial H^2}\frac{\partial^2 s}{\partial \kappa^2} - \frac{\partial^2 s}{\partial \kappa \partial H}\frac{\partial^2 s}{\partial \kappa \partial H} \right) \tag{4}$$
$$\sigma_{H\kappa} = 2\sigma_s \frac{\partial^2 s}{\partial H \partial \kappa} \Big/ \left(\frac{\partial^2 s}{\partial H^2}\frac{\partial^2 s}{\partial \kappa^2} - \frac{\partial^2 s}{\partial \kappa \partial H}\frac{\partial^2 s}{\partial \kappa \partial H} \right)$$

We can recover eq. (3) by making the cross-derivatives in eq. (4) equal to zero.

Even the more accurate expression (4) implicitly assumes that the stacking surface (eq. 1) is proportional to the true probability density for V_P/V_S and H. In truth, eq. (1) is a weighted average for H and V_P/V_S and, for this reason, we find it more appropriate to employ a bootstrap approach to estimate the uncertainties (e.g. Chevrot & Van der Hilst 2000). This approach was originally introduced by Efron & Tibshirani (1991) as a device for extending the root-mean-square error of the mean $\bar{x}$ of a data set $x = (x_1, x_2, \ldots, x_n)$,

$$\sigma_x = \left[\sum_{i=1}^{n} (x_i - \bar{x})^2 / n(n-1) \right]^{1/2} \tag{5}$$

to estimators other than the mean. A large number of new receiver functions data subsets is generated by randomly replicating the original data set with replacement. For each one of the data subsets, new estimates for H and V_P/V_S are obtained in exactly the same manner that they were obtained for the original data set. This implies recomputing the stacking surface (eq. 1) as many times as number of data subsets exists and, typically, we based our statistics on 200 bootstrap replications. The covariance matrix is then obtained by applying the standard formulae for the mean, variance and covariance to the bootstrap estimates. One immediate reward of this approach

is freedom from the bell-shaped curve assumptions during the traditional approach (Efron & Tibshirani 1991) that form the basis of eq. (4).

4 RECEIVER FUNCTIONS IN IBERIA

We now introduce the receiver functions obtained at several seismic stations located in the Iberian Peninsula (Fig. 1). The data were obtained at both temporary and permanent stations, so that different formats and frequency bands—and varying recording periods—were involved. A number of seismic stations were temporarily deployed in Spain and Portugal within the framework of the NARS-Europe (Nolet & Vlaar 1982) and NARS-ILIHA experiments, recording from 1983 to 1988 and from 1988 to 1989, respectively. These stations were equipped with Teledyne-Geotech sensors feeding Kinemetrics PDR-2 acquisition systems, resulting in a flat recording band between 10 and 1000 mHz (Nolet *et al.* 1986). Unfortunately, most of the stations from this network did not record enough teleseismic data, so that we only performed our analysis for selected stations. Three short-period stations (VAN2, POBL and EBRE), operated by the Institut d'Estudis Catalans, were also included in our analysis. These short-period stations are equipped with three unidirectional Ranger-SS1 sensors and IDS-3602A Terra-Technology acquisition units, the resulting transfer function being flat in the range 1–50 Hz. Two of these short-period stations, EBRE and POBL, have been temporarily upgraded with broad-band STS-2 sensors within the framework of the MIDSEA project (Van der Lee *et al.* 2001). The remaining stations investigated in this study were equipped with broad-band sensors, either STS-2 sensors (MLS, MTE, MAHO, CART, MELI and SFUC), STS-1 sensors (PAB), or CMG-3T sensors (CADI).

To deconvolve the vertical component from the horizontal components of the teleseismic waveforms and calculate our receiver function estimates, we employed the iterative time domain technique of Ligorría & Ammon (1999), because of its better performance with short-period records. To ensure success during the deconvolution process, those receiver functions that did not reproduce (receiver function convolved with vertical waveform) at least 85 per cent of the original radial waveform were rejected. We note that a short period recording band does not necessarily pose difficulties for obtaining valid receiver functions (Fig. 2; Julià *et al.* 1998). For each station, both radial and transverse receiver functions were plotted in a time–back azimuth representation. This representation proved useful in identifying laterally varying structures and for checking for a 3-D complex structure beneath the stations. As shown in Fig. 1, there

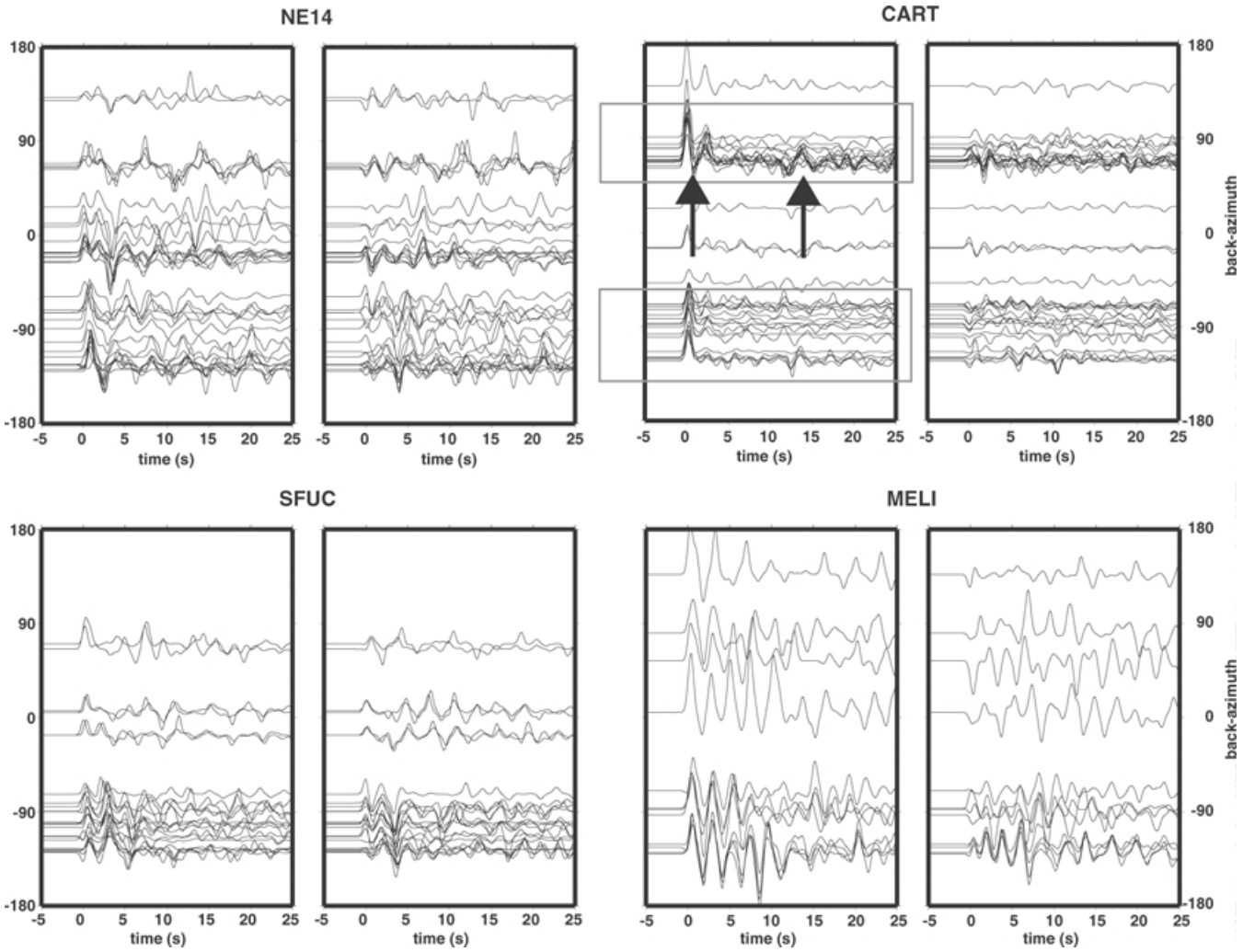

Figure 5. Radial and transverse receiver functions in the Betic Cordillera and the Alborán Basin. The rectangles indicate the range of backazimuths used in the H–κ stacking. The arrows point to specific features in the waveforms referenced in the text.

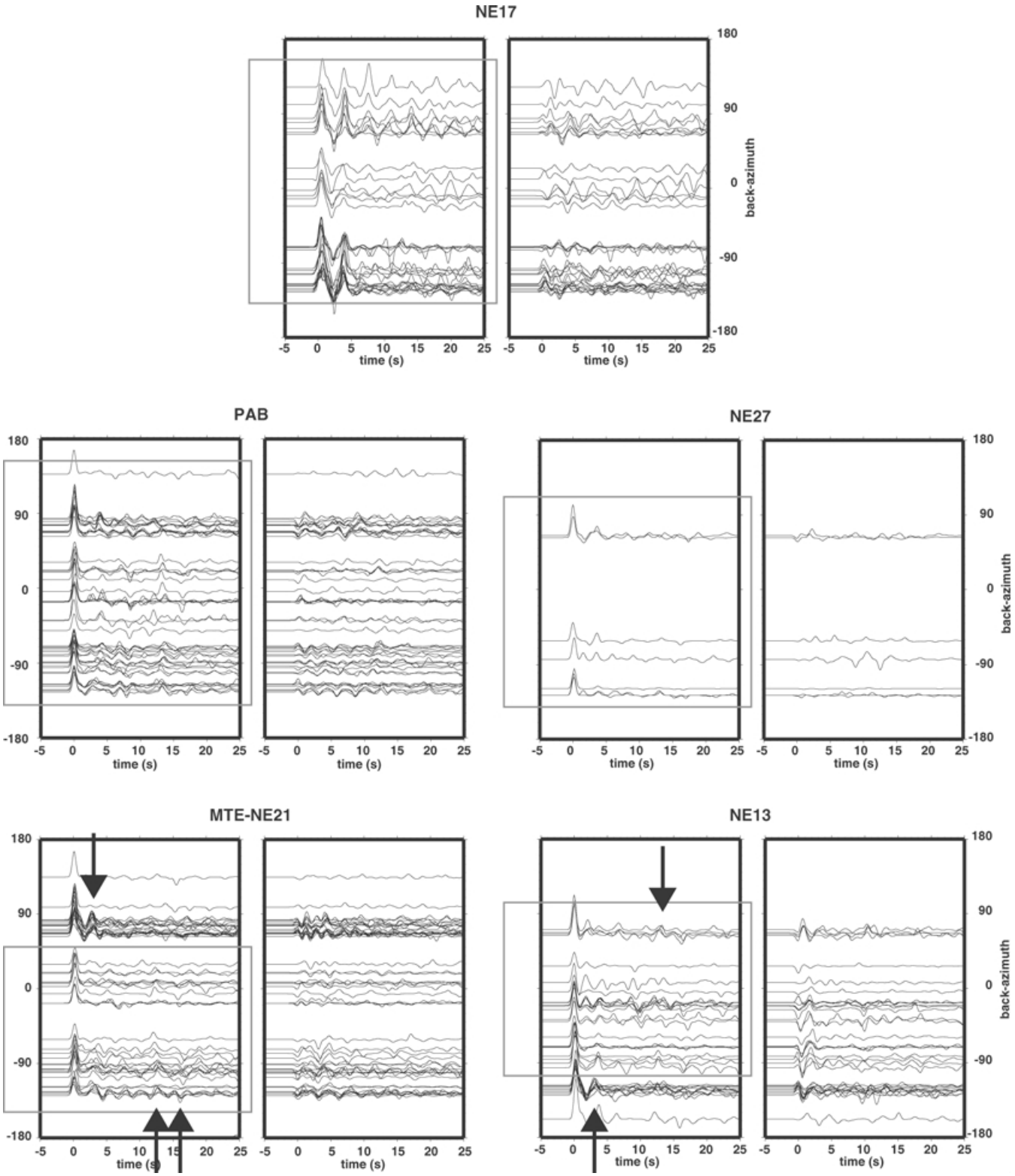

Figure 6. Radial and transverse receiver functions in the Iberian Massif. The rectangles indicate the range of backazimuths used in the H–κ stacking. The arrows point to Moho Ps and multiples in the waveforms.

are stations located at borders separating different tectonic units and the receiver response may then vary with the direction from which the teleseismic *P*-wave is approaching the station. In such cases, we found it more informative to perform the analysis separately for each receiver function pattern instead of stacking all the traces to obtain average estimates, as suggested by Zhu & Kanamori (2000).

Fig. 3 displays the radial and transverse receiver functions obtained at the Pyrenees (CADI, MLS) and the foreland Ebre Basin

(NE11, POBL). Station CADI displays significant amplitudes in the transverse receiver functions for events approaching the station from the east. The North Pyrenean Fault (NPF), which represents the collision margin between Iberia and Eurasia, has a complex geometry at depth (e.g. Muñoz 1992) and is most likely to be sampled by these events. The remaining waveforms for this station have less off-azimuth energy content and basically sample the Axial Zone, which is characterized by a crustal root of thickness up to 50 km (Gallart *et al.* 1981). At station MLS, we also observe significant transverse energy for events approaching the station parallel to the NPF, which strikes in an east–west direction. Events approaching from the north to this station sample the North Pyrenean Zone, a 33 km thick portion of European crust covered by Mesozoic sediments (Daignieres *et al.* 1981). The signature of this sedimentary cover is observed in the initial seconds of the radial waveforms, which display a small incident *P*-wave amplitude followed by a large Ps converted phase at the sediment–bedrock interface (Cassidy 1992; Zelt & Ellis 1998). Station POBL is located at the eastern edge of the Ebre Basin and limits with the Catalan Coastal Ranges. Julià *et al.* (1998) analysed the azimuthal pattern at this station and found that events approaching from the north across the basin had little transverse amplitudes, whereas events approaching from the north–east and south–west, along the CCR, had transverse amplitudes comparable to the corresponding radial amplitudes. Finally, *P*-waves approaching station NE11 from the north and east sample the western part of the Ebre Basin and display clear Moho Ps converted phases and small transverse amplitudes.

Stations sampling the Catalan Coastal Ranges (VAN2) and the València Trough (VAN2, MAHO, EBRE-NE25) also show interesting varying patterns (Fig. 4). Receiver functions at station VAN2, located between the CCR and the València Trough, displays different patterns depending on the on-shore/off-shore origin of the incoming *P*-wave. Note, for instance, how the peak at approximately 7 s in the western (on-shore) receiver functions is absent in the eastern (off-shore) waveforms. The crust in this region is supposed to thin very rapidly towards the Mediterranean margin, as a result of the extensional tectonics operating in the València Trough (e.g. Gallart *et al.* 1995). At station MAHO, at the opposing edge of the trough, teleseismic *P*-waves recorded for western azimuths also image the thinned crust in the trough, whereas the events approaching from the east sample the crust of the Algerian Basin. Note how the prominent peak at approximately 3 s in the waveforms sampling structure west of the station is not observed in the waveforms sampling structure east of the station. Station EBRE-NE25 is located in a small Neogen sedimentary basin by the Mediterranean coast (Julivert *et al.* 1977), and also displays different patterns according to the on-shore/off-shore incoming directions. The observed pattern, however, is likely to be attributed to reverberations in the basin geometry (note the ringing from 5 to 10 s in the western waveforms) rather than variations in crustal properties.

Fig. 5 displays the receiver functions obtained at stations CART, NE14, SFUC and MELI. Station NE14 is located next to the Crevillente fault (Fig. 1), which separates the Inner from the External Betics (see, e.g., Weijermars 1991). This station shows significant transverse energy at all azimuths, which is probably related to the complexity at depth of the fault and the high degree of deformation of the Betic crust, resulting from the Neogene collision. Conversely, station CART, located in the internal zone, does not show significant off-azimuth energy. Indeed, the crust sampled by station CART is supposed to be of a very different nature to that sampled by station NE14 (Banda & Ansorge 1980). The radial waveforms display again azimuthal dependence. Note, for instance, how the prominent trough right after the incoming *P*-wave peak and the peak at approximately 14 s in the eastern waveforms are not observed in the western waveforms. Station SFUC is located in the Atlantic edge of the Guadalquivir foreland basin, and the complexity observed in both radial and transverse waveforms are probably the combined effect of basin geometry complicated with a high-velocity contrast at the sediment–bedrock interface (González *et al.* 1998). The waveforms at station MELI, in North Africa, are also complicated, where the ringing and the *P*-wave peak delay resemble the signature of a sedimentary layer.

Stations sampling the Iberian Massif (NE17, PAB, NE13, NE27 and MTE-NE21) did not show, in general, evidence for heterogeneous 3-D structure (Fig. 6). Recall that this unit has been relatively unaffected by Mesozoic and Cenozoic orogenies. The only complications arise at station NE17, located in the Tajo Basin, where the ringing in the waveforms are indicative of the signature of a sedimentary cover. Stations PAB and NE27 have very small transverse signal and no evidence for azimuthal variation in the waveforms. Intriguing azimuthal patterns were observed at station MTE-NE21, although associated with little transverse energy: for the northern events, there is no trace of the Ps wave but the crustal multiples seem to arrive at the expected times; for the western events, the timing for the Ps is somewhat erratic and, again, the multiples seem to be in the right place. For the events approaching from the east, the corresponding receiver functions show a prominent arrival at relative traveltimes expected for the Ps converted wave, but there is no trace of the multiples, and a prominent trough at approximately 2 s is observed. This last pattern is also observed at station NE13, for events recorded in the 180° and 250° backazimuth range. A gradational crust–mantle transition could, of course, account for missing multiples, but explaining missing Ps converted phases is more challenging: a strongly gradational crust–mantle transition right beneath the recording station sampled by the Ps converted phase, combined with a sharper discontinuity away from the station sampled by the multiples might have the desired effect. Finally, the receiver functions at NE13 show some transverse energy, and the Ps and PpPmS

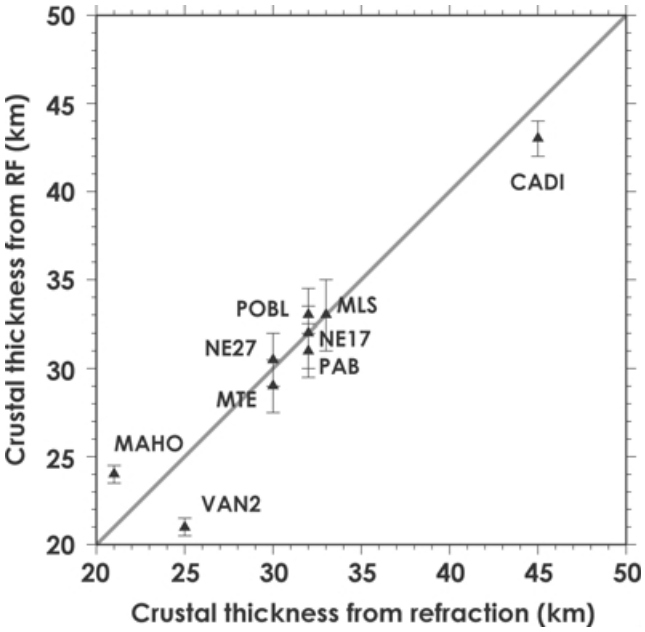

Figure 7. A comparison between crustal thicknesses from refraction/reflection surveys and our receiver function analysis. Confidence bounds correspond to a 2σ level.

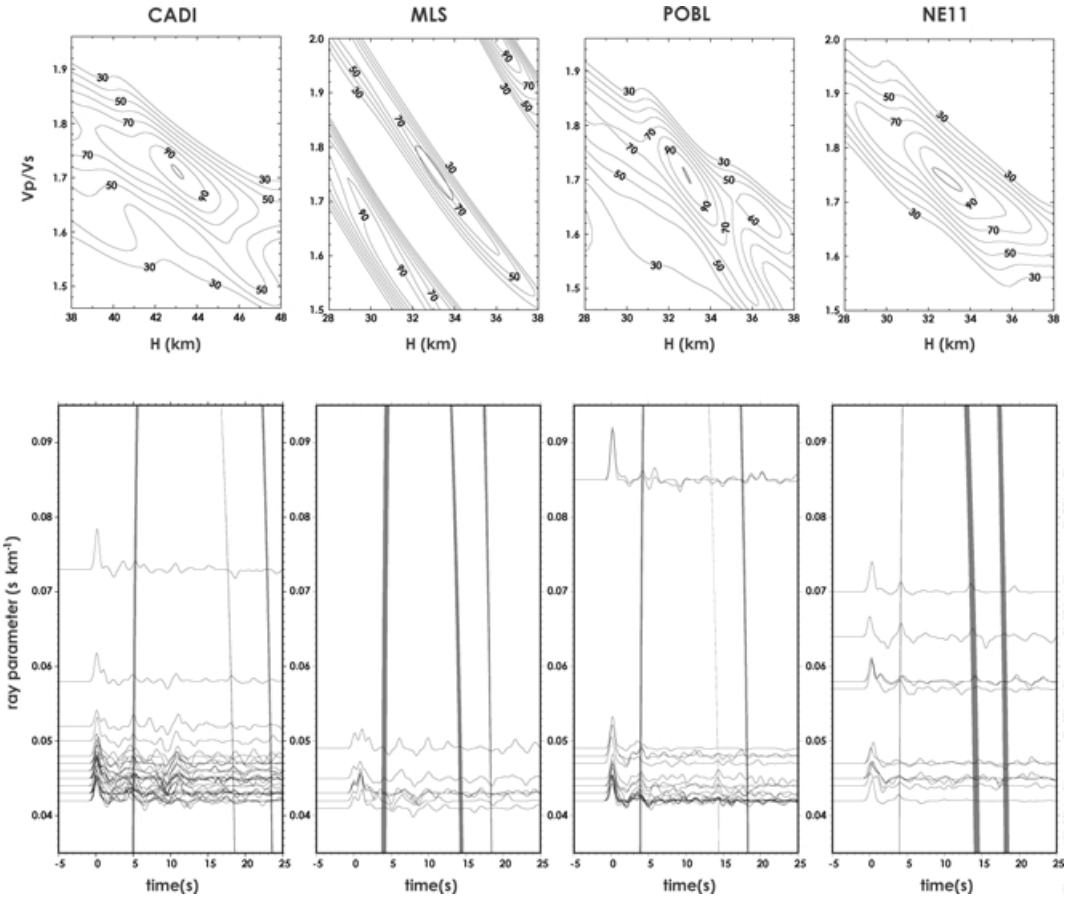

Figure 8. H–κ stacking analyses for the stations sampling the Pyrenees and its foreland basins. For each station the normalized stacking surface (normalized to 100 per cent) is shown on top. The confidence ellipse appears as a grey line overlapping the stacking surface. The phase matching for the receiver functions is shown at the bottom of each panel. The shadow zones are limited by the traveltimes given by $[H_{\max} - 2\sigma_H, (V_P/V_S)_{\max} + 2\sigma_{V_P/V_S}]$ and $[H_{\max} + 2\sigma_H, (V_P/V_S)_{\max} - 2\sigma_{V_P/V_S}]$. Note that the selected maximum at station MLS is a local maximum.

Moho interaction phases can be identified at approximately 4–5 and 12–13 s in the radial waveforms.

5 CRUSTAL THICKNESSES AND V_P/V_S RATIOS IN IBERIA

We applied the stacking procedure of Zhu & Kanamori (2000) to 11 seismic stations located in Spain and Portugal, and obtained 12 estimates for V_P/V_S and thickness of the Iberian crust (see Table 1). In general, independent *P*-wave velocities, which are a required input were obtained from previous refraction and reflection lines nearing the stations investigated. When this was not possible (stations NE11 and NE13) the values were extrapolated from seismic lines within the same tectonic unit. In general, the weights w_1, w_2 and w_3 in eq. (1) were given values of 0.4, 0.4 and 0.3, respectively, so that phases were weighted to have similar importance during the analysis. Confidence bounds were also obtained from a combination of 200 bootstrap replications (Efron & Tibshirani 1991). We checked the performance of the procedure by plotting the traveltimes corresponding to the maximum from the stacking surface against the receiver functions. This provided a visual check of the phases picked by the stacking algorithm and ensured an intuitively satisfying match between the estimates and the observations.

Table 1 is a list of the estimated values for H and V_P/V_S for each station and azimuthal group, along with 2σ confidence bounds, correlation factor, number of waveforms, assumed *P*-wave velocities and weights. Two standard deviation limits are considered in order to report values at a 95 per cent confidence level. In general, we observe that thicknesses are well constrained for all stations, with uncertainties ranging from ± 0.5 to ± 2.5 km, and that V_P/V_S are more variable with uncertainties ranging from ± 0.02 to ± 0.23. Larger uncertainties result when no Ps information is used, since multiply reverberated phases are generally less coherent as a result of its larger lateral sampling extent. The correlation coefficients between V_P/V_S and H are large and negative, as a result of the well-known depth–velocity trade-off for receiver functions. This implies that the estimated values for V_P/V_S and H do not vary independently within the uncertainty limits: the uppermost value for H within the uncertainty range will be coupled with the lowermost value for V_P/V_S and vice versa. Comparison with independent estimates of crustal thickness from refraction/reflection surveys is displayed in Fig. 7. The agreement between both data sets is indeed very good.

5.1 The Pyrenees and the Ebre Basin

Teleseismic *P*-waves approaching station CADI from the west and north and station MLS from the north sample the Axial and the northern domains of the Pyrenean mountain range, respectively. The Axial Zone is made of Iberian crust and is characterized by a crustal root which reaches 50 km in its central part (Gallart *et al.* 1981),

Region	*Station*	*Lat.* (deg)	*Lon.* (deg)	*Baz*	*# wvfr.*	*Vp* (km s^{-1})	*W1*	*W2*	*W3*	*Thick.* (km)	*Vp/Vs*	*Corr.* (%)
Pyrenean Range	CADI	42.3	1.8	N/W	52	6.2	0.5	0.5	0.0	43.0±1.0	1.71±0.03	-90.0
	MLS	43.0	1.1	N	7	6.2	0.0	0.5	0.5	33.0±2.0	1.75±0.10	-95.0
Ebre Basin	POBL	41.4	1.1	N	19	6.1	0.5	0.5	0.0	33.0±0.5	1.71±0.03	-97.5
	NE11	41.8	-1.5	N	12	6.2	0.5	0.5	0.0	33.0±1.5	1.74±0.04	-92.0
Catalan Coastal Ranges	VAN2	41.0	0.8	W	27	6.1	0.4	0.3	0.3	35.0±0.5	1.70±0.02	-94.5
Extensional Basins	MAHO	39.9	4.3	W	9	5.9	0.4	0.3	0.3	24.0±0.5	1.70±0.03	-90.5
	VAN2	41.0	0.8	E	12	5.7	0.5	0.5	0.0	21.0±0.5	1.74±0.02	-96.0
Iberian Massif	NE17	39.9	-4.1	all	35	6.2	0.0	0.5	0.5	32.0±2.5	1.88±0.23	-94.0
	PAB	39.5	-4.4	all	49	6.2	0.4	0.3	0.3	31.0±1.0	1.74±0.03	-92.0
	NE13	38.7	-4.1	N	23	6.2	0.4	0.3	0.3	30.0±1.0	1.73±0.04	-90.5
	NE27	38.5	-8.0	all	7	6.2	0.4	0.3	0.3	30.5±1.5	1.72±0.03	-78.0
	MTE-NE21	40.4	-7.5	N/W	29	6.2	0.0	0.5	0.5	29.0±1.5	1.76±0.08	-97.0

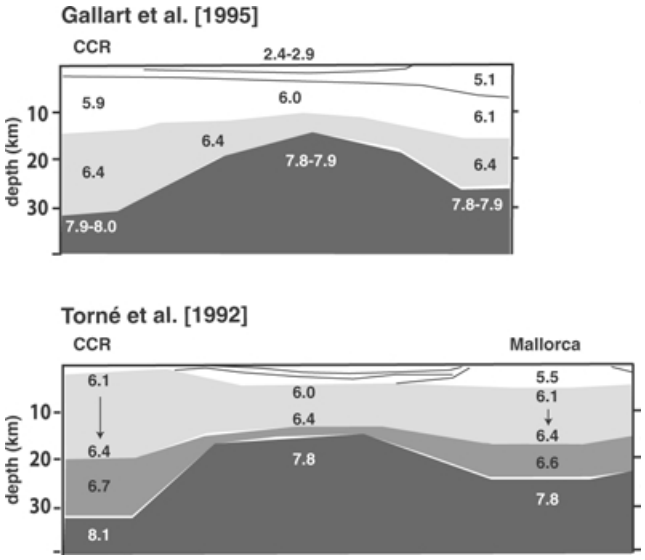

Figure 9. Two crustal models for the València Trough. Note the different *P*-wave velocity estimates for the upper and lower crusts.

whereas the North Pyrenean Zone is made of European crust with a thickness of approximately 33 km (Daignieres *et al.* (1981). The stacking procedure at these stations yields 43.0 ± 1.0 km and 1.71 ± 0.03 for the thickness and V_P/V_S ratio at station CADI, and 33.0 ± 2.0 km and 1.75 ± 0.10 for the thickness and V_P/V_S ratio at station MLS (Fig. 8). The thicknesses obtained beneath CADI and MLS with the stacking procedure are compatible with those reported by the refraction data. Daignieres *et al.* (1981) also reported crustal V_P/V_S ratios of 2.0 for the sedimentary layer and 1.73 for the crystalline basement in the North Pyrenean Zone. Because of these high V_P/V_S ratio sediments, the teleseismic *P*-wave multiples generated at the sediment–bedrock interface interfere with the Ps converted phase at the Moho. Thus, only the multiply reverberated phases at the base of the crust could be employed during the stacking analysis (Fig. 8). As a result, the V_P/V_S ratio is poorly constrained beneath station MLS, although a value of 1.75 seems a good estimate. The receiver function estimate for V_P/V_S beneath CADI could actually be a lower limit, since the Moho is thought to be dipping westward in this region (Gallart *et al.* 1981).

For the southern foreland basin—the Ebre Basin—stations POBL and NE11 provide crustal thicknesses of 33 ± 0.5 and 33 ± 1.5 km, and V_P/V_S ratios of 1.71 ± 0.03 and 1.74 ± 0.04, respectively (Fig. 8). Thickness estimates are in excellent agreement with refraction and reflection data (Torné *et al.* 1992; Gallart *et al.* 1995), and with a receiver function study at POBL (Julià *et al.* 1998). However, a receiver function study by Van der Meijde *et al.* (2003) in the Mediterranean–European region reports values of 28 ± 1 km for the thickness and 0.28 ± 0.02 for the Poisson ratio in this station. Recall that we employed receiver functions approaching station POBL from the north, only. Van der Meijde *et al.* (2003) stacked the receiver functions from all azimuths, so that their estimates most likely reflect a different average compared with the estimates reported in this study.

5.2 The València Trough and the Catalan Coastal Ranges

Stations VAN2, EBRE-NE25 and MAHO, located at the eastern coast of Iberia and Menorca Island, respectively, sampled thinned crust at opposing edges of the València Trough (Table 1). This is a rift basin formed because of the Neogene to Recent extensional tectonics that affected, in different ways, the western Mediterranean. The structure at depth of the trough has been imaged by a number of refraction and reflection experiments (Banda *et al.* 1980; Torné *et al.* 1992; Gallart *et al.* 1995). All the crustal models agree in that no oceanic crust has been created and in the asymmetric character of the trough, but differ in the details (Fig. 9). Gallart *et al.* (1995) reported thicknesses of 30 and 25 km for the Mediterranean and Balearic margins, respectively, and a 6.4 km s^{-1} lower crust. Torné *et al.* (1992) reports similar crustal thicknesses, but images the lower crust as a 6.6–6.7 km s^{-1} velocity layer. Also, the steepness of the Moho towards the centre of the trough from the Iberian and Balearic margins, respectively, is reversed in those models. Our analysis (Fig. 10) shows a thicker crust in the Balearic margin with

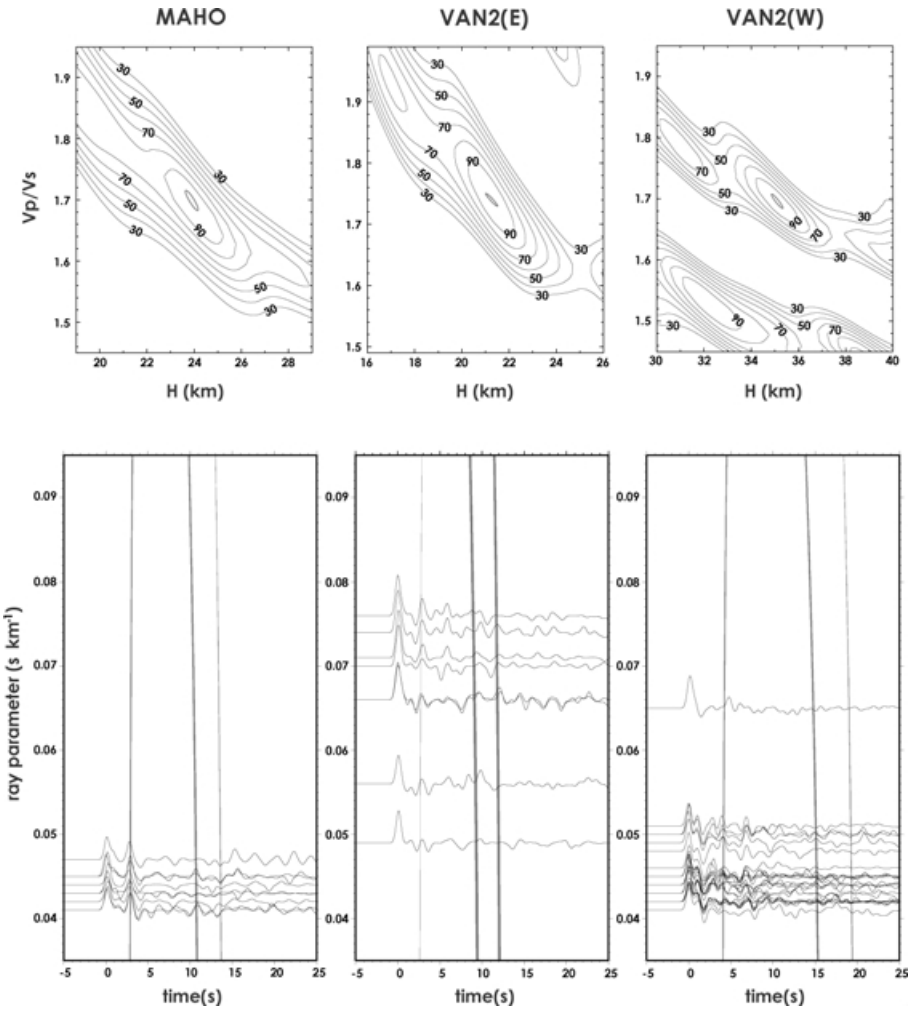

Figure 10. The same as in Fig. 8 for stations sampling the València Trough and Catalan Coastal Ranges. Note that the selected maximum at station VAN2(W) is a local maximum.

respect to the Iberian margin. Station EBRE-NE25 was not employed because the Moho interaction phases were not clearly identified in the waveforms (Fig. 4). The thickness at the Balearic margin is 24 ± 0.5 km and agrees well with the value reported in the reflection/refraction studies and with the value of 25 ± 1.3 km inferred by Van der Meijde *et al.* (2003). Our V_P/V_S ratio is 1.70 ± 0.03 which also agrees with the Poisson ratio of 0.24 ± 0.03 of Van der Meijde *et al.* (2003). In the Iberian margin, station VAN2 yields a thickness of 21 ± 0.5 km and a V_P/V_S ratio of 1.74 ± 0.02. These estimates, however, are likely to be affected by the dipping Moho and the finite extent of the lateral sampling of the receiver functions. Since the teleseismic *P*-waveforms recorded at VAN2 travel downdip, the V_P/V_S of 1.74 beneath VAN2 would be an overestimation of the true value.

Station VAN2 also sampled the Catalan Coastal Ranges with events approaching the station from the west (Fig. 1). In this case, we obtain a thickness of 35 ± 0.5 km and a V_P/V_S ratio of 1.70 ± 0.02 (Fig. 10). This implies a change in thickness of approximately 15 km at the opposing sides of this station. Indeed, Torné *et al.* (1992) imaged a decrease in crustal thickness of approximately 15 km within a horizontal distance of just 50 km (Fig. 9). Also, according to the heat flow map of Fernàndez *et al.* (1998), station VAN2 is close to a local minimum of heat flow (approximately 60 mW m^{-2}). Heat-flow is anticorrelated to crustal thickness (Bodri & Bodri 1985) so that a decrease in heat-flow implies an overall thicker crust.

5.3 The Betic Cordillera

Within the Betic Cordillera only station CART displayed small enough transverse energy to qualify for our stacking analysis. Unfortunately, we were unable to obtain any crustal thickness estimates, since station CART did not show multiply reverberated phases from the Moho in the radial receiver functions (Fig. 5). Banda & Ansorge (1980) interpreted the structure in the crust and upper-mantle from a 440 km length profile from Cartagena to Cádiz. The authors noted that the crust east of the Palomares fault (Fig. 1), with an average V_P of 6.3 km s^{-1} and a thickness of only 23 km, appears to be so different from the crust west of the fault system, which is approximately 5 km thicker and 0.3 km s^{-1} slower. Our receiver function data suggest that the crust–mantle transition is not as sharp as that suggested by the refraction models.

In the upper-mantle, Banda & Ansorge (1980) noted the presence of a 26 km thick low-velocity zone (LVZ) of 7.8 km s^{-1} underlying a 6 km thick high-velocity zone at the crust–mantle boundary with a strong gradient from 8.0 to 8.2 km s^{-1}. Mueller & Ansorge (1986) reinterpreted the profile and obtained a 27 km thick LVZ of 7.7 km s^{-1} with its bottom at 63 km depth. The velocity beneath the LVZ

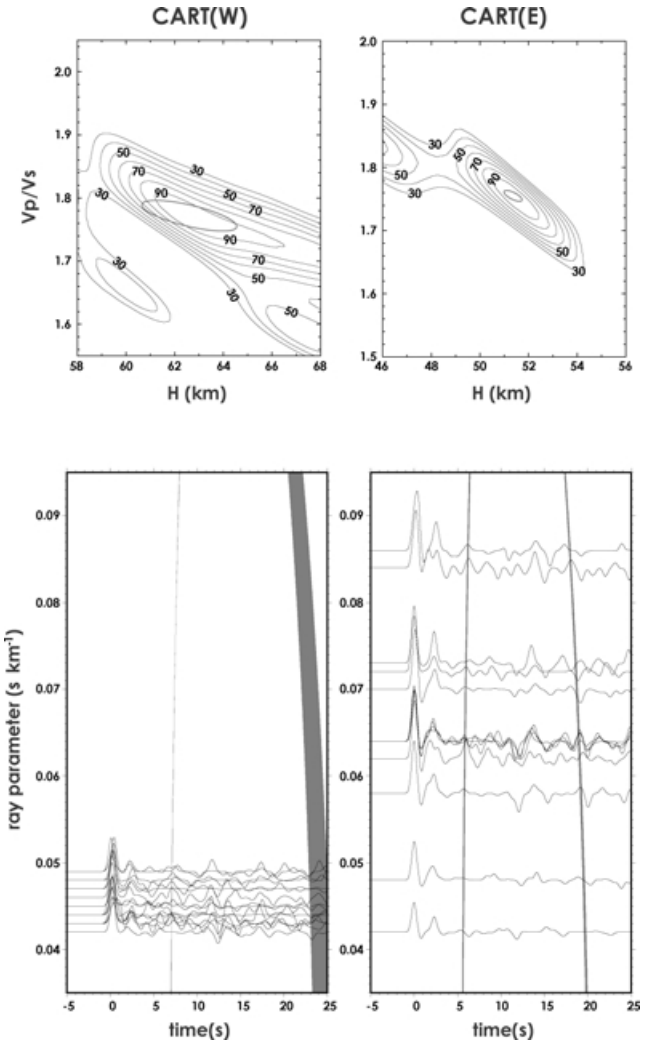

Figure 11. The same as in Fig. 8 for station CART (east and west) in South Eastern Spain.

was set to 8.3 km s^{-1} in both studies. We sought evidence for this LVZ by moving the thickness window in our stacking procedure to higher values and found a deep discontinuity at 62.5 ± 4.0 km depth west of station CART (Fig. 11). Moreover, a similar contrast was also observed at a shallower depth of 51.5 ± 1.0 km off the east coast (Fig. 11). The significance of this LVZ in the upper-mantle and its relation to the mantle under the Alborán Basin is not yet clear, but our analysis suggests that it extends to the east and that it has been affected by the rapid stretching of the lithosphere related to the opening of the Alborán Basin.

5.4 The Iberian Massif

Five of the stations investigated in this study sample the Iberian Massif (see Fig. 1), the Palaeozoic core of the Iberian Peninsula. Refraction profiling in the Massif reports thicknesses of 29–30 km in Portugal (Mendes-Victor *et al.* 1993) and thicknesses and V_P/V_S ratios of 30–31 km and 1.75, respectively, in the central Iberian Massif (Banda *et al.* 1981). The H–κ stacking analyses for these stations are shown in Fig. 12 and the resulting estimates are in good agreement with those reported by seismic profiling (Fig. 7). Comparison is also possible for a *P*-wave coda study carried out by Paulssen & Visser (1993), who reported thicknesses of 27 and 29 km beneath stations NE21 and NE17 (29 ± 1.5 and 32 ± 3.0 km in our study), respectively, which lie close to the edge of our confidence ellipses. Those estimates were based on just 6 and 3 events, respectively, so that the confidence bounds are presumably large. Receiver functions in the Iberian Massif were also analysed at station PAB by Sandvol *et al.* (1998) (34 ± 2.7 km for the crustal thickness) and by Van der Meijde *et al.* (2003) (32 ± 0.9 and 0.21 ± 0.02, for the thickness and the Poisson ratio, respectively), and our estimates are 31.0 ± 1.0 km and 1.74 ± 0.03 (a Poisson ratio of 0.24–0.26) (see Table 1). Note that the confidence bounds for the thickness estimates overlap in all cases except for those for the V_P/V_S value of Van der Meijde *et al.* (2003), which do not. However, a thickness of 32 km in our H–κ stacking surface would be associated to a V_P/V_S ratio of 1.71 (a Poisson ratio of 0.24), which is close to the 0.23 upper bound of Van der Meijde *et al.* (2003).

The average crustal thickness inferred from the stations sampling the Iberian Massif is 30 ± 2 km, this is a value lower than the 38 km expected from worldwide averages of Palaeozoic orogens (Zandt & Ammon 1995). A collection of seismic profiling information by Meissner (1986) shows that our value coincides with crustal thickness averages observed in other Variscan outcrops of the European continent. Further evidence of this anomalous thin crust is obtained from the average heat-flow of 71 ± 17 mW m^{-2} reported by Fernàndez *et al.* (1998) in the Iberian Massif, which is approximately 10 mW m^{-2} higher than expected for crust of Palaeozoic age (Pollack *et al.* 1993). Meissner *et al.* (1987) argued that these outcrops have lost their crustal roots by some sort of continental-wide process of rheologic flattening, involving accretion of terranes to existing continents and, perhaps, heating and differentiation of the lower crust (Meissner & Weber 1986). Wittenberg *et al.* (2000) also suggested the possibility of orogenic root delamination after collision, during the Variscan orogeny. An example of this unexpected flatness of the Moho has been reported by Carbonell *et al.* (2001) in a seismic reflection experiment in SW Iberia, where geological evidence for a major suture zone has been observed (Simancas *et al.* 2001).

The accretionary nature of the Iberian Massif has been studied by Quesada (1991), suggesting that the Iberian Massif is the result of the amalgamation of a number of exotic terranes to a Palaeozoic Iberian Autochton during the Variscan orogeny. Flattening by either heating and differentiation or delamination would imply the removal of mafic lower crust rocks, a more felsic composition and a lower than average V_P/V_S ratio of the Iberian Massif crust. Wittenberg *et al.* (2000) noted that seismic observations along the European Geotraverse Central segment indicate an overall felsic composition of the Variscan crust. The average V_P/V_S ratio in the Iberian Massif from our study is 1.74 ± 0.05 (station NE17 was not included in the average because of the large confidence bounds), which is close to the value of 1.75 obtained by Banda *et al.* (1981) in central Spain and includes the world average of 1.78 obtained by Zandt & Ammon (1995) for Palaeozoic crust. Unfortunately, seismic evidence for the removal of lower crustal rocks cannot be worked out from our data set, but the possibility remains.

6 CONCLUSIONS

We have introduced and analysed receiver function waveforms at 11 stations in the Iberian Peninsula and Balearic Islands. We have shown that the receiver function patterns correlate with the tectonic units of Iberia and we have provided 12 local measurements of H and V_P/V_S by employing the H–κ stacking technique of Zhu & Kanamori (2000). Our estimates are in good agreement with independent estimates from seismic profiling and independent receiver

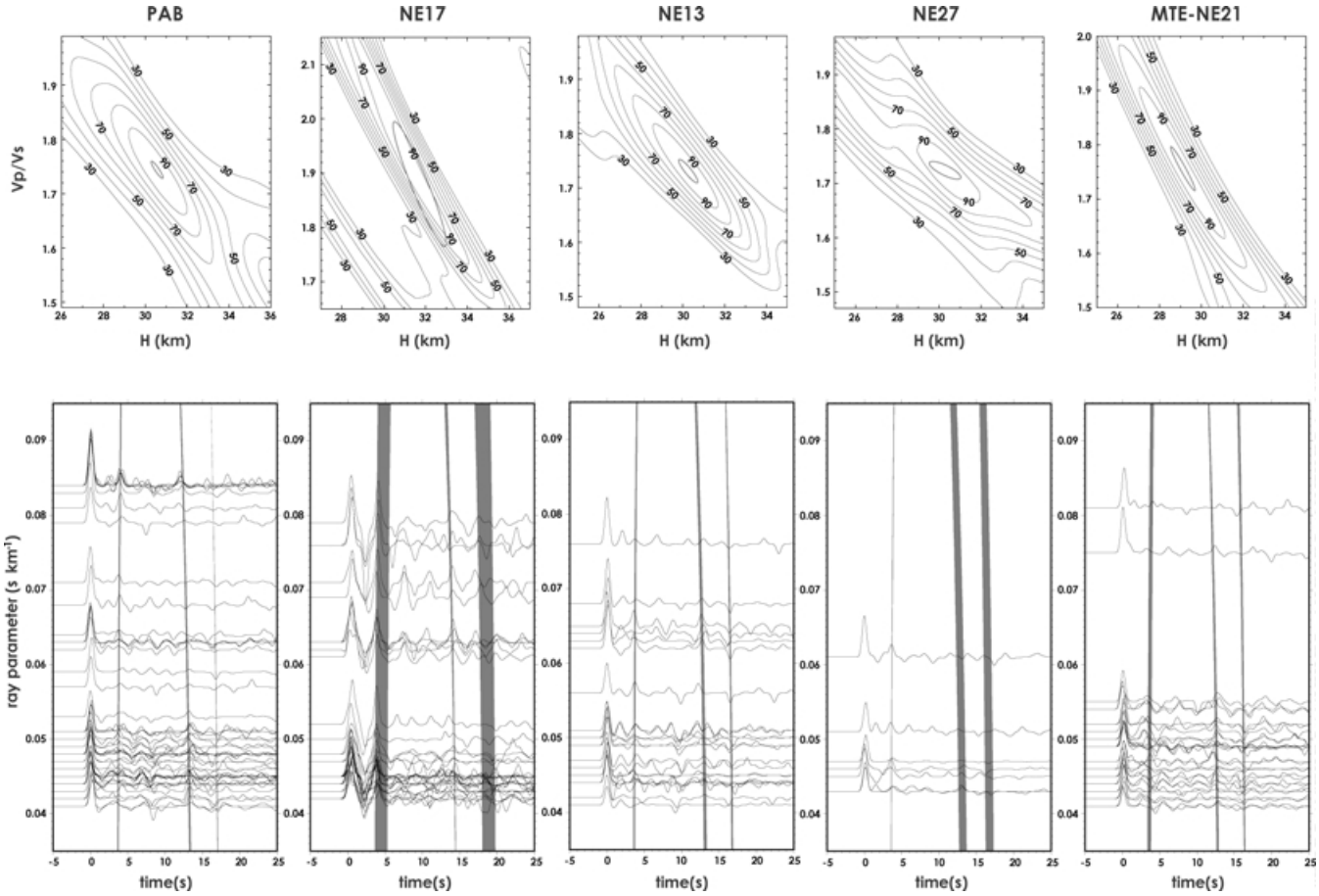

Figure 12. The same as in Fig. 8 for stations sampling the Iberian Massif and the Tajo Basin.

function and *P*-wave coda studies for the region. The crustal roots at the Betics, Pyrenees and Catalan Coastal Ranges, and the stretched crust in the València Trough have been clearly imaged by the receiver functions. Evidence for an uppermost mantle reflector in the Betics–Alborán region imaged by independent refraction profiles has also been found in our receiver function study. Further evidence for an anomalously thin crust in the Iberian Massif has been presented but evidence for thinning by removal of mafic lower crust rocks could not be assessed with the present data set.

ACKNOWLEDGMENTS

We wish to thank the following institutions for their role in the collection and sharing of seismic data: Institut d'Estudis Catalans, MIDSEA, Observatori de l'Ebre, GEOFON, NARS, ReNaSS and IRIS. Charles J. Ammon is also thanked for valuable comments, and Lupei Zhu and Susan Van der Lee are thanked for critically reviewing the manuscript. We acknowledge the Lawrence Livermore National Laboratory for their work on the Seismic Analysis Code (SAC) and Wessel & Smith (1998) for their work on the Generic Mapping Tools (GMT).

REFERENCES

Álvaro, M., Capote, R. & Vegas, R., 1979. Un modelo de evolución geotectónica para la Cadena Celtibérica, *Acta Geól. Hispánica,* **14,** 172–177.

Ammon, C.J., 1991. The isolation of receiver effects from teleseismic *P* waveforms, *Bull. seism. Soc. Am.,* **81,** 2504–2510.

Ammon, C.J., Randall, G.E. & Zandt, G., 1990. On the non-uniqueness of receiver function inversions, *J. geophys. Res.,* **95,** 15 303–15 318.

Banda, E., 1988. Crustal parameters in the Iberian Peninsula, *Phys. Earth planet, Inter.,* **51,** 222–225.

Banda, E. & Ansorge, J., 1980. Crustal structure under the central and eastern part of the Betic Cordillera, *Geophys. J. R. astr. Soc.,* **63,** 515–532.

Banda, E., Ansorge, J., Boloix M. & Córdoba, D., 1980. Structure of the crust and upper mantle beneath the Balearic Islands (western Mediterranean), *Earth planet. Sci. Lett.,* **49,** 219–230.

Banda, E., Suriñach, E., Aparicio, A., Sierra, J. & Ruiz de la Parte, E., 1981. Crust and upper mantle structure of the central Iberian Meseta (Spain), *Geophys. J. R. astr. Soc.,* **67,** 779–789.

Bodri, L. & Bodri, B., 1985. On the correlation between heat flow and crustal thickness, *Tectonophysics*, **120,** 69–81.

Carbonell, R., Simancas, F., Juhlin, C., Ayarza, P., González-Lodeiro, F., Pérez-Estaún, R., Plata, J. & IBERSEIS Working Group, 2001. IBERSEIS: a seismic reflection image of the Variscan orogen, SW Iberia, *EOS, Trans. Am. geophys. Un.,* **82,** 47.

Cassidy, J.F., 1992. Numerical experiments in broadband receiver function analysis, *Bull. seism. Soc. Am.,* **82,** 1453–1474.

Chevrot, S. & Van der Hilst, R.D., 2000. The Poisson ratio of the Australian crust: geological and geophysical implications, *Earth planet. Sci. Lett.,* **183,** 121–132.

Choukroune, P., 1992. Tectonic evolution of the Pyrenees, *Ann. Rev. Earth planet. Sci.,* **20,** 143–158.

Daignieres, M., Gallart, J. & Banda, E., 1981. Lateral variation of the crust in the North Pyrenean Zone, *Ann. Géophys.,* **37,** 435–456.

Dewey, J.F., Pitman, W.C., Ryan, W.B.F. & Bonnin, J., 1973. Plate tectonics and the evolution of the Alpine system, *Geol. Soc. Am. Bull.,* **84,** 3137–3180.

Efron, B. & Tibshirani, R., 1991. Statistical data analysis in the computer age, *Science,* **253,** 390–395.

Fernàndez, M., Marzán, I., Correia, A., Ramalho, E., 1998. Heat flow, heat production, and lithospheric thermal regime in the Iberian Peninsula, *Tectonophysics*, **291,** 29–53.

Gallart, J., Banda, E. & Daignieres, M., 1981. Crustal structure of the Paleozoic Axial Zone of the Pyrenees and transition to the North Pyrenean Zone, *Ann. Géophys.,* **37,** 457–480.

Gallart, J., Vidal, N. & Dañobeitia, J.J., 1995. Multichannel seismic image of the crustal thinning at the NE Iberian margin combining normal and wide angle reflection data, *Geophys. Res. Lett.,* **22,** 489–492.

González, A., Córdoba, D., Vegas, R. & Matias, L.M., 1998. Seismic crustal structure in the southwest of the Iberian Peninsula and the Gulf of Cádiz, *Tectonophysics*, **296,** 317–331.

Hoernle, K., Zhang, Y.-S. & Graham, D., 1995. Seismic and geochemical evidence for large-scale mantle upwelling beneath the eastern Atlantic and western and central Europe, *Science,* **374,** 34–39.

Julià, J., Vila, J. & Macià, R., 1998. The receiver structure beneath the Ebro Basin, Iberian Peninsula, *Bull. seism. Soc. Am.,* **88,** 1538–1547.

Julià, J., Herrmann, R.B., Ammon, C.J. & Akinci, A., 2003. Evaluation of deep sediment velocity structure in the New Madrid Seismic Zone, *Bull. seism. Soc. Am.,* (submitted).

Julivert, M., Fontboté, J.M., Ribeiro, A. & Conde, L., 1977. Mapa Tectónico de la Península Ibérica y Baleares, Instituto Geológico y Minero de España, Madrid.

Langston, C.A., 1979. Structure under Mount Rainier, Washington, inferred from teleseismic body waves, *J. geophys. Res.,* **84,** 4749–4762.

Ligorría, J.P., 2000. An investigation of the mantle–crust transition beneath North America and Poisson's ratio of the North American crust, *PhD thesis,* p. 261, Saint Louis Univ., Saint Louis.

Ligorría, J.P. & Ammon, C.J., 1999. Iterative deconvolution of teleseismic seismograms and receiver function estimation, *Bull. seism. Soc. Am.,* **89,** 1395–1400.

Meissner, R., 1986. *The Continental Crust: a Geophysical Approach,* Academic Press, San Diego.

Meissner, R. & Weber, Th., 1986. Nature and development of the crust according to deep reflection data from the German Variscides, in *Reflection Seismology: a Global Perspective,* eds Barazangi, M. & Brown, L.D., *AGU Geodyn. Ser.,* **13,** 31–42.

Meissner, R., Weber, Th. & Flüh, E.R., 1987. The Moho in Europe—implications for crustal development, *Ann. Geophysicae,* **5B,** 357–364.

Mendes-Victor, L.A., Miranda, J.M. & Marias, L.M., 1993. Crustal structure of Western Iberia from geophysical studies, in *Iberian Lithosphere Heterogeneity and Anisotropy,* 179–186, *Instituto Geográfico Nacional Monografía 10*.

Mueller, S. & Ansorge, J., 1986. Long-range seismic refraction profiles in Europe, in *Reflection Seismology: a Global Perspective,* eds Barazangi, M. & Brown, L.D., *AGU Geodyn. Ser.,* **13,** 167–182.

Muñoz, J.A., 1992. Evolution of a continental collision belt: ECORS-Pyrenees crustal balanced cross-section, in *Thrust Tectonics,* 235–246, ed. McClay, K.R., Chapman and Hall, New York.

Nolet, G. & Vlaar, N.J., 1982. The NARS project: probing the Earth's interior with a large seismic antenna, *Terra Cognita,* **2,** 17–25.

Nolet, G., Dost, B. & Paulssen, H., 1986. Intermediate wavelength seismology and the NARS experiment, *Ann. Geophys.,* **4,** 305–314.

Owens, T.J., Zandt, G. & Taylor, S.R., 1984. Seismic evidence for ancient rift beneath the Cumberland plateau, Tennessee: a detailed analysis of broadband teleseismic *P* waveforms, *J. geophys. Res.,* **89,** 7783–7795.

Paulssen, H. & Visser, J., 1993. The crustal structure in Iberia inferred from, *P*-wave coda, *Tectonophysics*, **221,** 111–123.

Pollack, H.N., Hurter, S.J. & Johnson, J.R., 1993. Heat flow from the Earth's interior: analysis of the global data set, *Rev. Geophys.,* **31,** 267–280.

Quesada, C., 1991. Geological constraints on the Paleozoic tectonic evolution of tectonostratigraphic terranes in the Iberian Massif, *Tectonophysics*, **185,** 225–245.

Sandvol, E., Seber, D., Calvert, A. & Barazangi, M., 1998. Grid search modeling of receiver functions: Implications for crustal structure in the Middle East and North Africa, *J. geophys. Res.,* **103,** 26 899–26 917.

Sanz de Galdeano, C.M., 1996. Tertiary tectonic framework of the Iberian Peninsula, in *Tertiary Basins of Spain, the Stratigrafic Record of Crustal Kinematics,* 9–14, eds Friend, P.F. & Dabrio, C.J., *World and Regional Geology 6,* Cambridge University Press, Cambridge.

Simancas, J.F., Martínez Poyatos, D., Expósito, I., Azor, A. & González Lodeiro, F., 2001. The structure of a major suture zone in the SW Iberian Massif: the Ossa-Morena/Central Iberian contact, *Tectonophysics*, **332,** 295–308.

Stich, D., Ammon, C.J. & Morales, J., 2003. Moment tensor solutions for small and moderate earthquakes in the Ibero-Maghreb region, *J. geophys. Res.,* **108,** 2148, doi:10.1029/2002JB002057.

Torné, M., Pascal, G., Buhl, P., Watts, A.B. & Mauffret, A., 1992. Crustal and velocity structure of the Valencia trough (western Mediterranean), Part I. A combined refraction/wide-angle reflection and near-vertical reflection study, *Tectonophysics*, **203,** 1–20.

Uchupi, E., 1988. The Mesozoic–Cenozoic geologic evolution of Iberia, a tectonic link between Africa and Europe, *Rev. Soc. Geol. España,* **1,** 257–294.

Van der Lee, S. *et al.*, 2001. Eurasia–Africa plate boundary region yields new seismographic data, *EOS, Trans. Am. geophys. Un.,* **82,** 637–645.

Van der Meijde, M., Van der Lee, S. & Giardini, D., 2003. Crustal structure beneath broadband seismic stations in the Mediterranean region, *Geophys. J. Int.* **152,** 729–739.

Vegas, R. & Banda, E., 1982. Tectonic framework and Alpine evolution of the Iberian Peninsula, *Earth Evol. Sci.,* **4,** 320–343.

Weijermars, R., 1991. Geology and tectonics of the Betic zone, SE Spain, *Earth Sci. Rev.,* **31,** 153–236.

Wessel, P. & Smith, W.H.F., 1998. New, improved version of the Generic Mapping Tools released, *EOS, Trans. Am. geophys. Un.,* **79,** 579.

Wittenberg, A., Vellmer, C., Kern, H. & Mengel, K., 2000. The Variscan lower continental crust: evidence for crustal delamination from geochemical and petrophyisical investigations, in *Orogenic Processes: Quantification and Modelling in the Variscan Belt,* eds Franke, W., Haak, V., Oncken, O. & Tanner, D., pp. 401–414, The Geological Society of London.

Zandt, G. & Ammon, C.J., 1995. Continental crust composition constrained by measurements of crustal Poisson's ratio, *Nature,* **374,** 152–154.

Zandt, G., Myers, S.C. & Wallace, T.C., 1995. Crust and mantle structure across the Basin and Range-Colorado Plateau boundary at 37°N latitude and implications for Cenozoic extensional mechanism, *J. geophys. Res.,* **100,** 10 529–10 548.

Zelt, B.C. & Ellis, R.M., 1998. Receiver function studies in the Trans-Hudson orogen, Saskatchewan, *Can. J. Earth Sci.,* **36,** 585–603.

Zhu, L. & Kanamori, H., 2000. Moho depth variation in southern California from teleseismic receiver functions, *J. geophys. Res.,* **105,** 2969–2980.